

$\pi^+p$  Interactions at 4 GeV/c

AACHEN-BERLIN-BIRMINGHAM-BONN-HAMBURG-LONDON (I.C.)-MÜNCHEN COLLABORATION\*

(Received 15 January 1965)

In photographs taken with the Saclay 81-cm hydrogen bubble chamber at the CERN proton synchrotron about 16 000  $\pi^+p$  scatterings at 4 GeV/c with two and four charged secondaries have been analyzed and identified. The cross sections for the individual two- and four-prong channels and for the production of resonances are given. The various effective-mass distributions are shown. The reaction  $\pi^+p \rightarrow p\pi^+\pi^0$  is dominated by  $N^{*++}$  and  $\rho^+$  production. From the reaction  $\pi^+p \rightarrow n\pi^+\pi^+$  the  $T=2$   $\pi\pi$  cross section as a function of the energy has been deduced applying the Chew-Low and the Selleri formula. The  $\pi\pi$  angular distribution is isotropic ( $s$  wave) up to  $\sim 800$  MeV. In the reaction  $\pi^+p \rightarrow p\pi^+(m\pi^0)$  the  $N^{*++}$  and the  $A_2^+$  occur. An estimate of the decay ratio  $A_2 \rightarrow \eta\pi/A_2 \rightarrow \rho\pi$  yielded  $0.3 \pm 0.2$ . About 75% of the reactions  $\pi^+p \rightarrow p\pi^+\pi^+\pi^-$  proceed via  $N^{*++}$  and  $\rho^0$  production. The major features of this reaction can be explained by the one-pion-exchange (OPE) model; the various distributions have been computed by a Monte Carlo method applying the Ferrari-Selleri off-shell corrections to the OPE formula. The experimental distributions can be reproduced rather well by the model. In the channel  $\pi^+p \rightarrow N^{*++}\pi^+\pi^-$  the angular-momentum state of the  $\pi^+\pi^-$  system has been studied. A highly pure sample of the reaction  $\pi^+p \rightarrow N^{*++}\rho^0$  has been obtained by limitation to small momentum transfers. A weak correlation between the  $N^{*++}$  and  $\rho^0$  decay angles is observed. In the  $\rho^0\pi^+$  effective-mass distribution the  $A_1$  and  $A_2$  show up. The  $A_1$  and  $A_2$  have a different  $\Delta^2$  and decay angular distribution; the  $A_1$  enhancement can perhaps be explained by the OPE model. In the  $p\pi^+\pi^-$  effective-mass distribution the  $T=\frac{1}{2}$  isobars at 1518 and 1688 MeV show up; there is no definite enhancement in the  $p\pi^+\pi^+$  mass distribution. From the reactions  $\pi^+p \rightarrow p\pi^+\pi^+\pi^-$  a highly pure sample of the channel  $\pi^+p \rightarrow N^{*++}\omega^0$  could be obtained by limitation to small  $\Delta^2$ . The  $B$  meson is present in the  $\omega^0\pi^+$  mass distribution; no definite conclusion for the spin and parity of the  $B$  meson could be reached. The previously observed enhancement at 975 MeV in the  $\rho\pi$  mass distribution is discussed further. In the reaction  $\pi^+p \rightarrow n\pi^+\pi^+\pi^-$  and in the four-prong reactions with several neutrals there is no strong resonance production except for a slight amount of  $N^*$  and  $\rho$ . Finally the  $\Delta^2$  distributions for six two-body reactions (elastic scattering and five channels with resonance production) are given and compared with each other. In all distributions a small accumulation of events at high  $\Delta^2$  is observed besides the strong peak at small  $\Delta^2$ .

## 1. INTRODUCTION

RECENTLY many investigations<sup>1-16</sup> on  $\pi p$  interactions have been made to study  $\pi$  and resonance production between 1.5 and 5 GeV/c (in the publications

\* Members of the collaboration are:

M. Aderholz, L. Bondár, W. Brauneck, and M. Deutschmann, Physikalisches Institut der Technischen Hochschule, Aachen, Germany.

C. Grote, H. Kaufmann, U. Kundt (Present address: The Joint Institute for Nuclear Research, Dubna, Russia), K. Lanius, R. Leiste, H. W. Meier, and R. Pose, Forschungsstelle für Physik hoher Energien der Deutschen Akademie der Wissenschaften zu Berlin-Zeuthen, Germany.

D. C. Colley, W. P. Dodd, B. Musgrave, and J. Simmons, Physics Department, University of Birmingham, Birmingham, England.

K. Böckmann, J. Moebes, B. Nellen, and G. Winter, Physikalisches Institut der Universität Bonn und KFA Jülich, Bonn, Germany.

V. Blobel, H. Butenschön, I. Dammann, P. v. Handel, E. Lohrmann, P. Schilling, M. W. Teucher, and G. Wolf, Physikalisches Staatsinstitut, II. Institut für Experimentalphysik, Hamburg and DESY, Hamburg, Germany.

J. M. Brownlee, I. Butterworth (present address: University of California, Berkeley, California), F. I. Campaigne, M. Ibbotson (present address: University of Manchester, Manchester, England), and M. Saeed, Physics Department, Imperial College, London, England.

N. N. Biswas, K. Gottstein, D. Lüers, P. Schlamp, N. Schmitz, J. Weigl, and W. Wittek, Max-Planck-Institut für Physik und Astrophysik, München, Germany.

<sup>1</sup> N. P. Samios, A. H. Bachmann, R. M. Lea, T. E. Kalogeropoulos, and W. D. Shepard, Phys. Rev. Letters **9**, 139 (1962).

<sup>2</sup> L. B. Auerbach, T. Elioff, W. B. Johnson, J. Lach, C. E. Wiegand, and T. Ypsilantis, Phys. Rev. Letters **9**, 173 (1962).

<sup>3</sup> C. Alif, D. Berley, D. Colley, N. Gelfand, U. Nauenberg, D. Miller, J. Schultz, J. Steinberger, T. H. Tan, H. Brugger, P. Kramer, and R. Plano, Phys. Rev. Letters **9**, 322 (1962).

<sup>4</sup> Saclay-Orsay-Bari-Bologna Collaboration, Nuovo Cimento

referred to, further references can be found). The British-German Collaboration has studied  $\pi^-p$  and  $\pi^+p$  interactions at a momentum of 4 GeV/c. Results for the  $\pi^-p$  interactions have already been published<sup>16</sup> and also some important details of the  $\pi^+p$  experiment.<sup>17</sup> In this paper we give a comprehensive re-

29, 515 (1963); Proceedings of the 1964 International Conference on High Energy Physics at Dubna (to be published); Nuovo Cimento **35**, 1 (1965).

<sup>5</sup> D. D. Carmony, F. Grard, R. T. Van de Walle, and N. Xuong, Proceedings of the 1962 International Conference on High Energy Physics at CERN (CERN, Geneva, 1962), p. 44.

<sup>6</sup> V. Hagopian and W. Selove, Phys. Rev. Letters **10**, 533 (1963).

<sup>7</sup> M. Abolins, R. L. Lander, W. A. W. Mehliop, N. Xuong, and P. M. Yager, Phys. Rev. Letters **11**, 381 (1963).

<sup>8</sup> M. Abolins, D. D. Carmony, D. N. Hoa, R. L. Lander, C. Rindfleisch, and N. Xuong, Phys. Rev. **136**, B195 (1964).

<sup>9</sup> G. Goldhaber, J. L. Brown, S. Goldhaber, J. A. Kadyk, B. C. Shen, and G. H. Trilling, Phys. Rev. Letters **12**, 336 (1964).

<sup>10</sup> G. Goldhaber, Proceedings of the Conference on Particle and High Energy Physics at Boulder, 1964 (to be published).

<sup>11</sup> Y. Y. Lee, B. P. Roe, D. Sinclair, and J. C. Van der Velde, Phys. Rev. Letters **12**, 342 (1964).

<sup>12</sup> S. U. Chung, O. I. Dahl, L. M. Hardy, R. I. Hess, G. R. Kalbfleisch, J. Kirz, D. H. Miller, and G. A. Smith, Phys. Rev. Letters **12**, 621 (1964).

<sup>13</sup> P. H. Satterblom, W. D. Walker, and A. R. Erwin, Phys. Rev. **134**, B207 (1964).

<sup>14</sup> G. Puppi, Ann. Rev. Nucl. Sci. **13**, 287 (1963).

<sup>15</sup> S. S. Yamamoto, J. R. Smith, D. C. Rahm, and J. J. Lloyd, Proceedings of the 1964 International Conference on High Energy Physics at Dubna (to be published).

<sup>16</sup> Aachen-Birmingham-Bonn-Hamburg-London-München Collaboration: (a) Phys. Letters **5**, 153 (1963); (b) **5**, 209 (1963); (c) Nuovo Cimento **31**, 485 (1964); (d) **31**, 729 (1964).

<sup>17</sup> Aachen-Berlin-Birmingham-Bonn-Hamburg-London-München Collaboration: (a) Phys. Letters **10**, 226 (1964); (b) **10**, 229 (1964); (c) **10**, 240 (1964); (d) **10**, 248 (1964); (e) **11**, 167 (1964); (f) Nuovo Cimento **34**, 495 (1964); (g) **35**, 659 (1965).

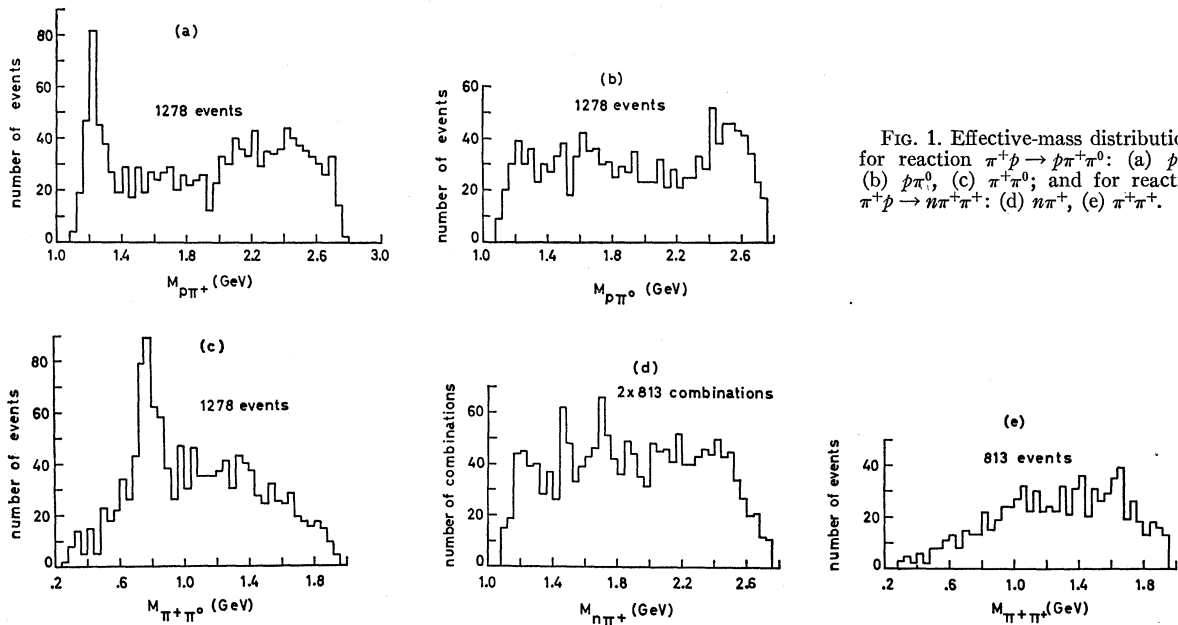


FIG. 1. Effective-mass distributions for reaction  $\pi^+p \rightarrow p\pi^+\pi^0$ : (a)  $p\pi^+$ , (b)  $p\pi^0$ , (c)  $\pi^+\pi^0$ ; and for reaction  $\pi^+p \rightarrow n\pi^+\pi^+$ : (d)  $n\pi^+$ , (e)  $\pi^+\pi^+$ .

port on reactions with two and four charged secondary tracks.

The experiment has been carried out at the CERN proton synchrotron using a separated  $\pi^+$  beam. The momentum spread of the beam was about  $\pm 1\%$ . This beam was directed into the Saclay 81-cm hydrogen bubble chamber. During the exposure about 70 000 good pictures were taken.

For the selection of events a fiducial region 30 cm long and 20 cm wide has been applied, assuring a minimum track length of 35 cm for secondary tracks going in the forward direction.

Among the approximately 16 000 events which were scanned and measured, about 2% could not be analyzed due to measuring difficulties. The analysis was carried out in the usual fashion using geometrical reconstruction and kinematical fitting programs. An event was taken to fit a given hypothesis if its  $\chi^2$  probability for that hypothesis was acceptable. In addition to the fitting the ionization density of the secondary tracks was used for identification. It was possible to distinguish by

ionization between proton and  $\pi^+$  up to a momentum of about 1.5 GeV/c. After use of the ionization density approximately 3% of the events turned out to fit more than one hypothesis. For these events the hypothesis with the highest  $\chi^2$  probability has been taken.

Those events which did not give an acceptable fit to any hypothesis were assumed to have more than one neutral secondary particle. They were classified further, if possible, by means of the ionization density, leaving of the total about 9% ambiguous two-prong events and about 2% ambiguous four-prong events with several neutrals. These ambiguous events were not used in the study of the no-fit channels.

In order to standardize and to check the identification and measuring procedures a sample of 20 events was

TABLE I. Numbers of events and cross sections.

Channel	No. of events analyzed	Corrected cross section in mb
(1) $p\pi^+$	3289	6.42
(2) $p\pi^+\pi^0$	1376	2.31
(3) $n\pi^+\pi^+$	862	1.44
(4) $p\pi^+(m\pi^0), m \geq 2$	1813	3.04 (3.32)
(5) $n\pi^+\pi^+(m\pi^0), m \geq 1$	1064	1.78 (2.88)
ambiguous (4) or (5)	827	1.38
Total two-prongs	9231	16.37
(6) $p\pi^+\pi^+\pi^-$	2132	3.09
(7) $p\pi^+\pi^+\pi^-\pi^0$	2363	3.43
(8) $n\pi^+\pi^+\pi^+\pi^-$	639	0.93
(9) $p\pi^+\pi^+\pi^-(m\pi^0), m \geq 2$	872	1.27 (1.33)
(10) $n\pi^+\pi^+\pi^+\pi^-(m\pi^0), m \geq 1$	488	0.70 (0.87)
ambiguous (9) or (10)	161	0.23
Total four-prongs	6655	9.65

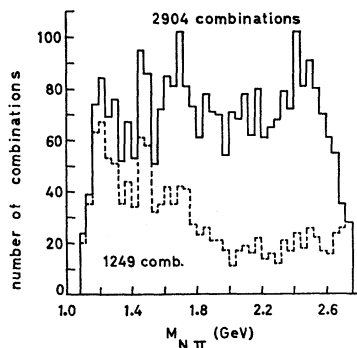


FIG. 2. Sum of the nucleon-pion effective-mass distributions for  $p\pi^0$  from reaction  $\pi^+p \rightarrow p\pi^+\pi^0$  and  $n\pi^+$  from reaction  $\pi^+p \rightarrow n\pi^+\pi^+$  (both combinations). Events with  $\Delta^2(p/N\pi) < 0.6$  GeV<sup>2</sup> are shown by the dashed histogram.

processed by all groups and the results were compared.

The kinematical quantities for the analyzed events were punched on cards which were used as input for our calculation and plotting program.

## 2. CROSS SECTIONS

Table I gives the total numbers of events and the cross sections for each channel. The cross sections were obtained by normalizing the total number of events (including six-prong and strange-particle events and the various corrections) to the total cross section of 28.00 mb given by Citron *et al.*<sup>18</sup> for this momentum. (The total cross section has not been determined from the data of this experiment, since the contamination of the  $\pi^+$  beam was not very well known.)

In the case of the elastic cross section a 16.5% correction has been made for the scanning loss of events at small scattering angles.<sup>17(d)</sup>

In order to get a rough estimate of how the small fraction of ambiguous no-fit events has to be divided between the two no-fit channels, a comparison of momentum and angular distributions with corresponding distributions for reactions where  $\pi^0\pi^0$  is replaced by a  $\pi^+\pi^-$  pair has been carried out. From this comparison the cross sections in brackets have been obtained.

## 3. TWO-PRONG EVENTS

### A. Elastic Scattering

The elastic-scattering reaction (1) has been discussed previously.<sup>17(d)</sup> The diffraction peak could be fitted by an exponential of the form  $e^{At}$  with  $A = (7.26 \pm 0.22)$  GeV<sup>-2</sup>. There was also evidence for backward scattering.

### B. Resonance Production

Figure 1 shows the effective-mass distributions for the reactions

$$(2) \quad \pi^+p \rightarrow p\pi^+\pi^0$$

and

$$(3) \quad \pi^+p \rightarrow n\pi^+\pi^+.$$

Partial cross sections for resonance production are given in Table II; they were determined by estimating the numbers of events in the resonance regions of the effective-mass plots above background. As it is impossible to determine accurately the background levels for wide resonances, the quoted cross sections are uncertain by about  $\pm 20\%$ .

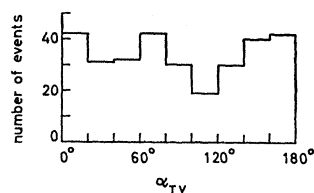


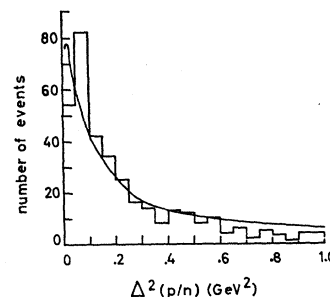
FIG. 3. Treiman-Yang angular distribution for reaction  $\pi^+p \rightarrow n\pi^+\pi^+$  with  $\Delta^2(p/n) < 0.3$  GeV<sup>2</sup>.

<sup>18</sup> A. Citron, W. Galbraith, T. F. Kycia, B. A. Leontic, R. H. Phillips, and A. Rousset (to be published).

FIG. 4.  $\Delta^2(p/n)$  distribution for reaction

$$\pi^+p \rightarrow n\pi^+\pi^+$$

with  $M_{\pi^+\pi^+} < 2.0$  GeV<sup>2</sup>. The curve is proportional to  $\Delta^2/(\Delta^2 + \mu^2)^2$  and is normalized to the experimental histogram between  $0.1$  GeV<sup>2</sup>  $< \Delta^2(p/n) < 0.5$  GeV<sup>2</sup>.



Reaction (2) is characterized by  $\rho^+$  and  $N^{*++}$  formation. The two reactions

$$(2a) \quad \pi^+p \rightarrow p\rho^+,$$

$$(2b) \quad \pi^+p \rightarrow N^{*++}\pi^0,$$

have been discussed in previous publications<sup>17(b),(f)</sup> in terms of the Stodolsky-Sakurai<sup>19</sup> and Gottfried-Jackson-Pilkun<sup>20-22</sup> analyses. In the framework of the absorp-

TABLE II. Partial cross sections for reactions (2) and (3).

Channel	$\sigma$ (mb)
$p\rho^+$	0.35
$N^{*++}\pi^0$	0.3
$p\pi^+\pi^0$ (direct channel)	1.55
$N^{*++}\pi^+$ ( $N^{*+} \rightarrow p\pi^0, n\pi^+$ )	0.2
$n\pi^+\pi^+$ (direct channel)	1.35

tive model the density matrix elements for the  $\rho^+$  in reaction (2a) are in good agreement with the predictions of Gottfried and Jackson<sup>22</sup> for pure  $\pi$  exchange. The  $N^{*++}$  decay distributions for reaction (2b) were found to agree completely with the predictions for  $\rho$  exchange.

The  $p\pi^0$  and  $n\pi^+$  effective-mass distributions of Fig. 1 both show some evidence for production of the nucleon isobars. Figure 2 gives the sum of the two distributions;

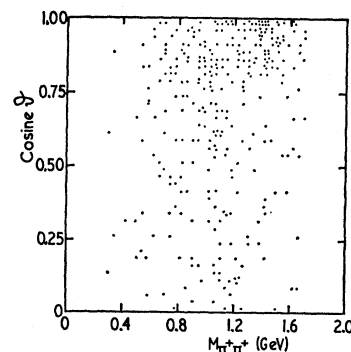


FIG. 5. Scatter diagram of the cosine of the angle  $\vartheta$  between incoming and outgoing  $\pi^+$  in the  $\pi^+\pi^+$  system versus the  $\pi^+\pi^+$  effective mass for reaction  $\pi^+p \rightarrow n\pi^+\pi^+$  with  $\Delta^2(p/n) < 0.3$  GeV<sup>2</sup>.

<sup>19</sup> L. Stodolsky, and J. J. Sakurai, Phys. Rev. Letters **11**, 90 (1963).

<sup>20</sup> K. Gottfried and J. D. Jackson, Nuovo Cimento **33**, 309 (1964).

<sup>21</sup> J. D. Jackson and H. Pilkun, Nuovo Cimento **33**, 906 (1964).

<sup>22</sup> K. Gottfried and J. D. Jackson, Nuovo Cimento **34**, 735 (1964).

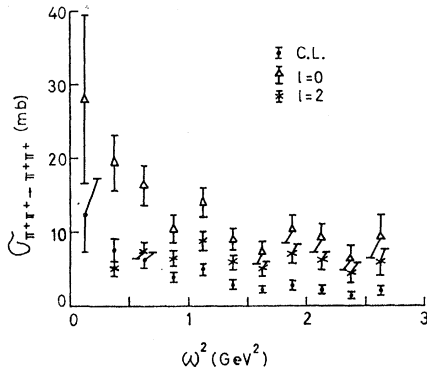


FIG. 6. Cross section for  $\pi^+\pi^+ \rightarrow \pi^+\pi^+$  as a function of total  $\pi^+\pi^+$  energy squared, obtained from Chew-Low formula ( $\bullet$ ), from the Selleri formula with  $l=0$  ( $\Delta$ ) and  $l=2$  ( $\times$ ), applied to  $\pi^+p \rightarrow n\pi^+\pi^+$  with  $\Delta^2(p/n) < 0.3 \text{ GeV}^2$ .

events with square  $\Delta^2(p/N\pi)$  of 4-momentum transfer between incoming proton and  $N\pi$  system less than  $0.6 \text{ GeV}^2$  are displayed in the dashed histogram. In addition to the  $\frac{3}{2}, \frac{3}{2}$  isobar there also appears to be some indication for the  $T=\frac{1}{2}$  isobars at 1518 and 1688 MeV.

### C. $T=2 \pi\pi$ Cross Section

In reaction (3) the two pions are in a pure  $T=2$  state, and if the reaction is dominated by one-pion exchange (OPE) one should be able to deduce the  $T=2 \pi\pi$  scattering cross section. Figure 3 shows the distribution of the Treiman-Yang angle for events with square of 4-momentum transfer between incoming proton and outgoing neutron,  $\Delta^2(p/n) < 0.3 \text{ GeV}^2$ . The distribution is consistent with isotropy, which is expected for OPE. As a further check we have plotted in Fig. 4 the  $\Delta^2(p/n)$  distribution (up to  $1 \text{ GeV}^2$ ) for the reactions (3) with  $\omega^2 \equiv M_{\pi^+\pi^+}^2 < 2.0 \text{ GeV}^2$ . The curve shows the prediction  $\Delta^2/(\Delta^2 + \mu^2)^2$  of the Chew-Low formula<sup>23</sup> normalized to the experimental histogram. (Due to the cutoff in  $\omega^2$ , the integration of the Chew-Low formula over  $\omega^2$  gives a factor independent of  $\Delta^2$ .)

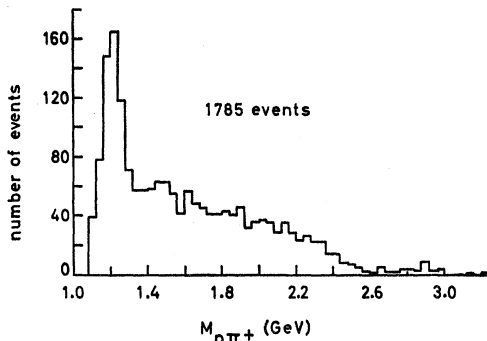


FIG. 7.  $p\pi^+$  effective-mass distribution for reaction  $\pi^+p \rightarrow p\pi^+(m\pi^0, m \geq 2)$ .

<sup>23</sup> G. F. Chew and F. E. Low, Phys. Rev. **113**, 1640 (1959).

Figure 5 shows a plot of the cosine of the scattering angle  $\vartheta$  between incoming and outgoing  $\pi^+$  in the  $\pi^+\pi^+$  c.m. system versus the mass  $M_{\pi^+\pi^+}$ , again for  $\Delta^2(p/n) < 0.3 \text{ GeV}^2$ . Since the two secondary  $\pi^+$  are indistinguishable, the one going in the forward direction was always taken ( $\cos\vartheta > 0$ ). For  $T=2 \pi\pi$  scattering only  $l=0, 2, 4, \dots$  partial waves contribute. For low energies ( $M_{\pi^+\pi^+} \leq 0.8 \text{ GeV}$ ),  $s$ -wave scattering seems to be dominant.

The  $\pi^+\pi^+$  scattering cross section as a function of the square of the total c.m.  $\pi^+\pi^+$  energy  $\omega^2$  has been deduced in the usual way by inserting the experimental values for  $d\sigma/d\omega^2$  into the theoretical expression obtained by intergrating the formula for  $d^2\sigma/d\omega^2 d\Delta^2$  over  $\Delta^2$ . The computation has been carried out first using the Chew-Low formula which is strictly valid only at the pion pole; second, using the Selleri modification<sup>24</sup> of the Chew-Low formula for  $s$ -wave  $\pi\pi$  scattering; and third, using the Selleri modification for  $d$ -wave scattering. In each case the integration has been carried out up to three different cutoff values for  $\Delta^2$ : 0.3, 0.5, and 1.0  $\text{GeV}^2$ . For each formula the results obtained for these three different cutoffs in  $\Delta^2$  were practically the same, except for the value at the lowest  $\omega^2$ , which increased with increasing  $\Delta^2$  cutoff. Figure 6 shows the resulting  $\pi^+\pi^+$  cross section as a function of  $\omega^2$  for the three different cases and for the lowest  $\Delta^2$  cutoff value, namely,  $0.3 \text{ GeV}^2$ .

The values for  $\sigma_{\pi^+\pi^+}$  obtained by using the Chew-Low formula are in good agreement with those previously deduced from the reaction  $\pi^-p \rightarrow N^*\pi^+\pi^-$  at<sup>25</sup> 4  $\text{GeV}/c$  and at<sup>4</sup> 2.75  $\text{GeV}/c$  and also with those recently obtained<sup>4</sup> from the reaction  $\pi^+p \rightarrow n\pi^+\pi^+$  at 2.75  $\text{GeV}/c$ . It is seen from Fig. 6 that the values obtained with the Selleri formula are larger than the Chew-Low values.

### D. No-Fit Events

Figure 7 shows the  $p\pi^+$  mass distribution for those reactions (4) where the proton could be definitely identified by ionization. The  $\frac{3}{2}, \frac{3}{2}$  isobar shows up

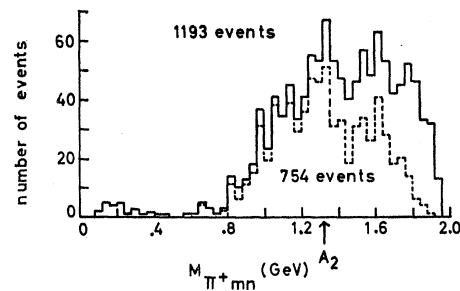


FIG. 8. Effective-mass distribution of  $\pi^+$  combined with missing neutrals (mn) for reaction  $\pi^+p \rightarrow p\pi^+(m\pi^0, m \geq 2)$ , with  $M_{p\pi^+}$  outside  $N^*$  region (1.12 to 1.32  $\text{GeV}$ ). Events with  $\Delta^2(p/p) < 0.6 \text{ GeV}^2$  are shown by the dashed histogram.

<sup>24</sup> F. Selleri, Phys. Letters **3**, 76 (1962).

<sup>25</sup> N. Schmitz, Nuovo Cimento **31**, 255 (1964).

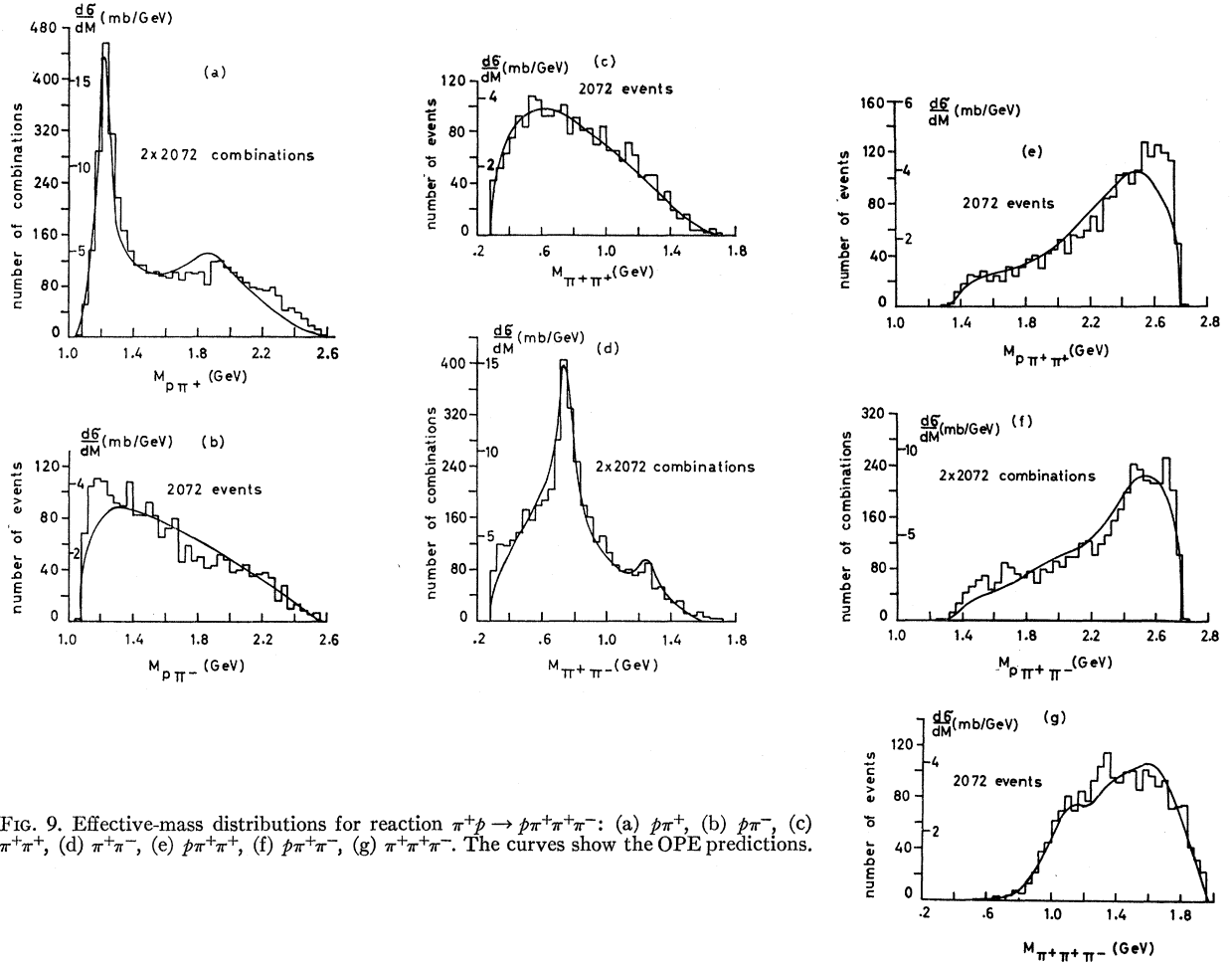


FIG. 9. Effective-mass distributions for reaction  $\pi^+p \rightarrow p\pi^+\pi^+\pi^-$ : (a)  $p\pi^+$ , (b)  $p\pi^-$ , (c)  $\pi^+\pi^+$ , (d)  $\pi^+\pi^-$ , (e)  $p\pi^+\pi^+$ , (f)  $\pi^+\pi^+\pi^-$ , (g)  $\pi^+\pi^+\pi^-$ . The curves show the OPE predictions.

prominently. As already has been pointed out,<sup>17(a)</sup> the missing mass distribution for this sample of reactions (4) shows the production of the  $\eta$  meson. The number of events in the  $\eta$  peak is consistent with what one expects from the number of  $\eta$  mesons decaying into charged particles [Fig. 28(h)] and the known branching ratio  $R(\eta \rightarrow \text{all neutrals})/R(\eta \rightarrow \text{charged}) \approx 2.0$ .

In order to search for decays of positively charged pion resonances into  $\pi^+$ +neutrals, we have plotted in Fig. 8 the appropriate effective-mass distribution for reactions (4) with  $M_{p\pi^+}$  outside the  $N^*$  region (1.12 to 1.32 GeV). Events with  $\Delta^2(p/p) < 0.6$  GeV<sup>2</sup> are shown by the dashed histogram. Although there are rather large statistical fluctuations, both distributions show a peak around 1320 MeV, the mass of the  $A_2$  meson, whereas the  $A_1$  meson does not show up. Thus there is evidence that the  $A_2$  does decay into  $\pi^+$ +neutrals ( $\eta^0\pi^+$  and  $\rho^+\pi^0$ ). For those events of Fig. 8 which are in the  $A_2$  region and for events in the two adjacent regions on the left and right sides we have plotted the missing-mass distributions. By comparing the number of  $\eta$  mesons appearing in these two distributions we have tried to determine the fraction of  $A_2$  mesons decaying into  $\eta^0\pi^+$ .

Taking into account the various decay modes of the  $\eta$  and the  $\rho^0\pi^+$  decay mode of the  $A_2$  we estimate that the ratio  $R$  of  $A_2$  decaying into  $\eta\pi$  to  $A_2$  decaying into  $\rho\pi$  ( $\rho^0\pi^+$  and  $\rho^+\pi^0$ ) is

$$R = \Gamma(A_2 \rightarrow \eta\pi) / \Gamma(A_2 \rightarrow \rho\pi) = 0.3 \pm 0.2.$$

Neither the  $\pi^+\pi^+$  not the missing-mass distribution for reactions (5) show any structure.

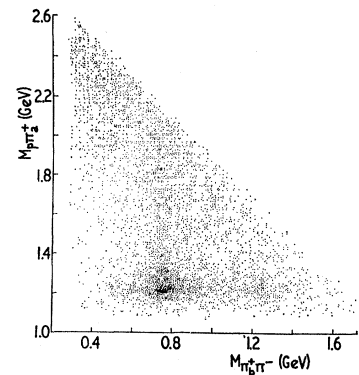


FIG. 10. Scatter diagram of  $M_{p\pi^+}$  versus  $M_{\pi^+\pi^-}$  (2 points per event) for reaction  $\pi^+p \rightarrow p\pi^+\pi^+\pi^-$ .

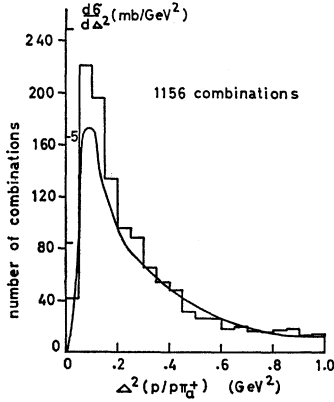


FIG. 11. Distribution of the momentum transfer  $\Delta^2(p/p\pi_a^+)$  for reaction  $\pi^+p \rightarrow p\pi^+\pi^+\pi^-$  with 1.12 GeV  $< M_{p\pi_a^+} < 1.32$  GeV. If both  $M_{p\pi_a^+}$  were in the  $N^*$  region, both  $\Delta^2$  have been plotted. The curve shows the OPE prediction.

#### 4. REACTION $\pi^+p \rightarrow p\pi^+\pi^+\pi^-$

##### A. Effective-Mass Distributions and Cross Sections

Figure 9 shows all effective-mass distributions for the reaction

$$(6) \quad \pi^+p \rightarrow p\pi^+\pi^+\pi^-.$$

The curves in these distributions will be discussed later. The partial cross sections for this channel are given in Table III. The over-all cross sections for  $N^{*++}$  (1.8 mb) and  $\rho^0$  (1.25 mb) production have been obtained from the effective-mass distributions. The cross sections for simultaneous production of two resonances have been obtained from the appropriate two-dimensional mass plot (Fig. 10) by computing the excess of events in the region where the two resonances overlap. These overlap regions were chosen wide enough to include the events in the tails of the resonances. Because of the difficulty of estimating the background in case of double-resonance production, the quoted values have been larger uncertainties (about  $\pm 30\%$ ) than the values for single-resonance production (about  $\pm 20\%$ ).

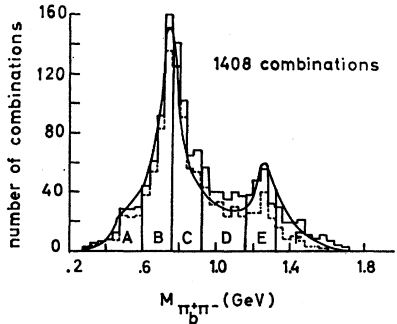


FIG. 12.  $\pi_b^+\pi^-$  effective-mass distribution for reaction  $\pi^+p \rightarrow p\pi^+\pi^+\pi^-$  with 1.12 GeV  $< M_{p\pi_a^+} < 1.32$  GeV. If both  $M_{p\pi_a^+}$  were in the  $N^*$  region both  $M_{\pi_b^+\pi^-}$  have been plotted. The dashed histogram shows events with  $\Delta^2(p/p\pi_a^+) < 0.75$  GeV $^2$ . The curve shows the OPE prediction. Definition of regions A to F: A, below 0.60 GeV; B, 0.60 to 0.76 GeV; C, 0.76 to 0.92 GeV; D, 0.92 to 1.16 GeV; E, 1.16 to 1.32 GeV; F, above 1.32 GeV.

TABLE III. Partial cross sections for reaction (6).

Channel	$\sigma$ (mb)
(a) $p\pi^+\pi^+\pi^-$ (no resonances)	0.4
(b) $N^{*++}\pi^+\pi^-$	1.1
(c) $N^{*++}\rho^0$	0.6
(d) $N^{*++}f^0$ ( $f^0 \rightarrow \pi^+\pi^-$ )	0.1
(e) $N^{*0}\pi^+\pi^+$	0.25
(f) $p\pi^+\rho^0$	0.65
$p\pi^+\rho^0$ (no $\rho\pi$ resonance)	0.3
$pA_1^+$	0.1
$pA_2^+$	0.25

##### B. $N^{*++}$ Production

It is clear from Fig. 9 that reaction (6) is dominated by  $N^{*++}$  and  $\rho^0$  production. This is also demonstrated by Fig. 10, which shows a scatter diagram of  $M_{p\pi_a^+}$  versus  $M_{\pi_b^+\pi^-}$ . For each event there appear two points, one of which is a background point if reaction (6) proceeds peripherally with one  $\pi^+$  going with the proton and the other one going with the  $\pi^-$ . It is seen from Fig. 9(a) that the ratio of  $N^*$  production to background under the  $N^*$  peak is about 3 to 1. Thus in order to obtain a pure sample of events for which  $\pi_a^+$  and proton are associated we now limit ourselves to events with  $M_{p\pi_a^+}$  in the  $N^*$  region (1.12 to 1.32 GeV). In the following these events will be called  $N^*$  events. Amongst the 1288  $N^*$  events there were 120 events for which both  $p\pi^+$  masses lie in the  $N^*$  region ("double  $N^*$  events"). Figure 11 shows the distribution of  $\Delta^2(p/p\pi_a^+)$  for  $N^*$  events up to 1 GeV $^2$ ; for double  $N^*$  events both  $\Delta^2$  values have been plotted. The graph shows the strong peripheral nature of the  $N^{*++}$  production mechanism.

##### C. $\pi_b^+\pi^-$ System for $N^*$ Events

Figure 12 shows the distribution of  $M_{\pi_b^+\pi^-}$  for  $N^*$  events; for "double  $N^*$  events," against both  $\pi^+\pi^-$  combinations have been taken. Events with  $\Delta^2(p/p\pi_a^+) < 0.75$  GeV $^2$  are shown by the dashed histogram. The mass spectrum is dominated by the  $\rho$  meson, but there is also an enhancement in the  $f^0$  region.

In order to study the angular-momentum state of the  $\pi\pi$  system, in Figs. 13 and 14  $\cos\theta$  and  $\varphi$  (Treiman-Yang angle) have been plotted versus  $M_{\pi_b^+\pi^-}$  for  $N^*$  events. The angles are defined by

$$\cos\theta = \frac{\pi_{in}^+ \cdot \pi_b^+}{|\pi_{in}^+||\pi_b^+|},$$

$$\cos\varphi = \frac{\mathbf{p}_{in} \times \mathbf{N}^* \cdot \pi_{in}^+ \times \pi_b^+}{|\mathbf{p}_{in} \times \mathbf{N}^*| |\pi_{in}^+ \times \pi_b^+|},$$

$$\sin\varphi = \frac{\pi_{in}^+ \times (\mathbf{p}_{in} \times \mathbf{N}^*) \cdot \pi_{in}^+ \times \pi_b^+}{|\pi_{in}^+ \times (\mathbf{p}_{in} \times \mathbf{N}^*)| |\pi_{in}^+ \times \pi_b^+|},$$

where all momenta are to be taken in the  $\pi_b^+\pi^-$  c.m.

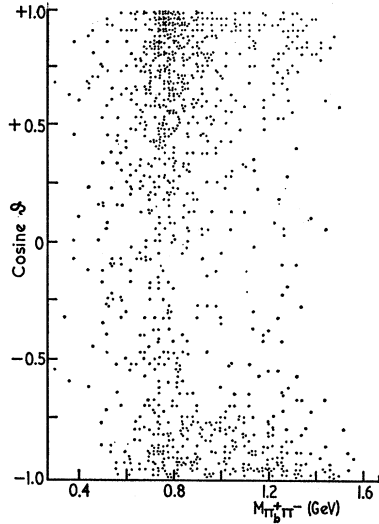


FIG. 13. Scatter diagram of the cosine of the angle  $\vartheta$  between incoming  $\pi^+$  and outgoing  $\pi_b^+$  in the  $\pi_b^+\pi^-$  c.m. system versus  $M_{\pi_b^+\pi^-}$  for reaction  $\pi^+p \rightarrow p\pi^+\pi^+\pi^-$  with  $1.12 \text{ GeV} < M_{p\pi_a^+} < 1.32 \text{ GeV}$  and  $\Delta^2(p/p\pi_a^+) < 0.75 \text{ GeV}^2$ .

system. Only events with  $\Delta^2(p/p\pi_a^+) < 0.75 \text{ GeV}^2$  have been taken. The distribution of  $\varphi$  is essentially isotropic for all dipion masses as expected for OPE. The  $\cos\vartheta$  distributions for the various  $\pi_b^+\pi^-$  mass regions defined in the caption to Fig. 12 are exhibited in Fig. 15. There appears a systematic trend from rough isotropy at low mass values to a forward-backward peaking at higher masses; the  $\rho^0$  shows its usual preference for forward peaking, but between the  $\rho^0$  and  $f^0$  regions the distribution becomes slightly backward-peaked, the backward peaking increasing through the  $f^0$  region.

For low  $\Delta^2(p/p\pi_a^+)$  and for OPE (see below)  $\vartheta$  represents the  $\pi\pi$  scattering angle. In order to attempt a determination of the angular-momentum states involved, we have fitted the distributions of Fig. 15 to

$$\frac{dN}{d \cos \vartheta} = \sum_{\nu=0}^n A_{\nu} \cos^{\nu} \vartheta.$$

For  $\pi\pi$  masses below  $\sim 0.9 \text{ GeV}$  good fits were obtained

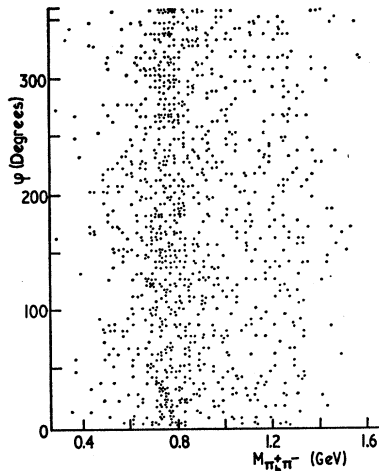


FIG. 14. Scatter diagram of Treiman-Yang angle  $\varphi$  versus  $M_{\pi_b^+\pi^-}$  for reaction  $\pi^+p \rightarrow p\pi^+\pi^+\pi^-$  with  $1.12 \text{ GeV} < M_{p\pi_a^+} < 1.32 \text{ GeV}$  and  $\Delta^2(p/p\pi_a^+) < 0.75 \text{ GeV}^2$ .

with  $n=2$  (i.e.,  $s$  and  $p$  waves); for higher masses it seemed necessary to go up to  $n=4$ , i.e., to include the  $d$  wave. The coefficients  $A_{\nu}$  and the  $\chi^2$  values obtained from the fitting are tabulated in Table IV. The experimental values for the asymmetry parameter  $R = (F-B)/(F+B)$  are also given in this table. The results for  $R$  are in good agreement with the compilation given by the Saclay-Orsay-Bari-Bologna collaboration<sup>26</sup> for the process  $\pi^-p \rightarrow n\pi^+\pi^-$ .

D.  $\pi^+p \rightarrow N^{*++}\rho^0$

As demonstrated in the two preceding sections there is a large amount of the reaction

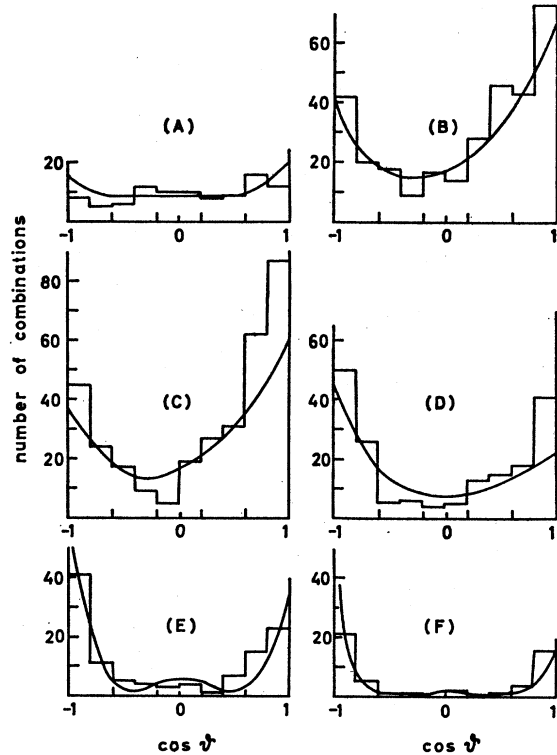
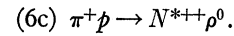


FIG. 15. Projection of Fig. 13 for the  $M_{\pi_b^+\pi^-}$  regions defined in Fig. 12. The curves show the OPE predictions.

Because of the peripheral nature of this reaction it should be possible to obtain a pure sample of it by selecting events with low  $\Delta^2(p/p\pi_a^+)$ . Figure 16 shows  $M_{p\pi_a^+}$  versus  $M_{\pi_b^+\pi^-}$  for  $\Delta^2(p/p\pi_a^+) < 0.3 \text{ GeV}^2$ . For those few events for which both  $\Delta^2$  were  $< 0.3 \text{ GeV}^2$ , that  $p\pi^+$  combination which gave the smaller  $\Delta^2$  has been taken. The projection of  $M_{p\pi_a^+}$  for the  $\rho$  band (0.66 to 0.86 GeV) of Fig. 16 and the projection of  $M_{\pi_b^+\pi^-}$  for the  $N^*$  band are shown in Fig. 17. In this way an almost pure sample of reaction (6c) was

<sup>26</sup> Saclay-Orsay-Bari-Bologna collaboration, Nuovo Cimento 35, 713 (1965).

TABLE IV. Coefficients  $A_i$  of polynomial in  $\cos\vartheta$ .

Region of Fig. 12	$A_0$	$A_1$	$A_2$	$A_3$	$A_4$	$\chi^2$	$(F-B)/(F+B)$
A	$12.1 \pm 1.8$	$4.1 \pm 2.1$	$-1.3 \pm 3.9$			2.6	$0.15 \pm 0.10$
B	$19.0 \pm 2.5$	$24.9 \pm 4.4$	$59.5 \pm 7.5$			4.1	$0.32 \pm 0.05$
C	$13.6 \pm 2.3$	$30.4 \pm 4.5$	$83.5 \pm 8.1$			11.2	$0.39 \pm 0.05$
D	$6.4 \pm 2.0$	$14.1 \pm 5.1$	$11.4 \pm 19.2$	$-28.9 \pm 11.3$	$66.3 \pm 26.0$	2.8	$0.01 \pm 0.07$
E	$3.4 \pm 1.3$	$1.9 \pm 4.6$	$1.0 \pm 13.5$	$-11.3 \pm 10.4$	$62.1 \pm 20.4$	5.4	$-0.12 \pm 0.09$
F	$1.5 \pm 0.8$	$1.1 \pm 1.9$	$-15.2 \pm 6.2$	$-3.6 \pm 5.0$	$44.3 \pm 9.7$	1.5	$-0.10 \pm 0.14$

obtained. This sample was used in a Gottfried-Jackson analysis reported in Ref. 17(g). The results of this analysis also indicated that reaction (6c) proceeds via pure  $\pi$  exchange, in agreement with the previous discussion.

Goldhaber<sup>10</sup> has reported strong correlations between the  $N^{*++}$  and  $\rho^0$  decay angles for this reaction. In order to search for these effects in our experiment we have plotted in Fig. 18 the cosine of the  $\rho$  decay angle  $\vartheta$  versus the cosine of the  $N^*$  decay angle  $\Theta$  for events in the  $N^*\rho$  overlap region of Fig. 16. Figure 19 shows projections of this scatter diagram for the  $\cos\Theta$  and  $\cos\vartheta$  regions chosen by Goldhaber. In order to make the comparison easier we show the same distributions in Fig. 20 all normalized to the same area. Within the statistics we do not observe a dependence of the  $\rho$  decay angle on the  $N^*$  decay angle. However, the  $N^*$ -decay angular distribution shows a tendency similar to that observed by Goldhaber although the effect is weaker than his. The effects observed in our experiment might perhaps be due to a small amount of residual background or to absorption.<sup>22</sup> A plot of the azimuth angle  $\varphi$  for  $\rho$  decay versus  $\Phi$  for  $N^*$  decay was more or less uniformly populated and did not show any correlation.

### E. OPE Calculations

In view of the peripheral nature of reaction (6) it is tempting to try to describe the principal features of this reaction quantitatively by the OPE diagram of Fig. 21. A theoretical formulation of the OPE model applicable to reaction (6) has been given by Ferrari and Selleri.<sup>27</sup> For the diagram of Fig. 21 they give the

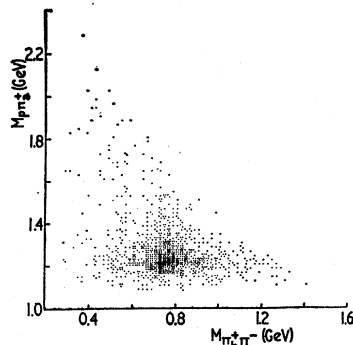


FIG. 16. Scatter diagram of  $M_{p\rho a^+}$  versus  $M_{\pi_b^+\pi^-}$  for reaction

$\pi^+ p \rightarrow p \pi^+ \pi^-$   
with  $\Delta^2 (p/p\pi_{a^+}) < 0.3 \text{ GeV}^2$ . If both  $\Delta^2$  were  $< 0.3 \text{ GeV}^2$  the  $\pi^+$  with the smaller  $\Delta^2$  has been taken to be  $\pi_{a^+}$ .

following expression which takes into account off-shell effects:

$$\frac{d^5\sigma}{d\Delta^2 dV^2 dW^2 d\cos\vartheta d\cos\Theta} = \frac{1}{16\pi^3} \frac{1}{q^2 s} \frac{|F(\Delta^2)|^2}{(\Delta^2 + \mu^2)^2} k_V V g_V(V, \Delta^2) \frac{d\sigma_V}{d\cos\vartheta} \times k_W W g_W(W, \Delta^2) \frac{d\sigma_W}{d\cos\Theta}. \quad (1)$$

The symbols in this and the subsequent expressions have the following meanings:  $m$  is the nucleon mass;  $\mu$  is the pion mass;  $M^*$  is the isobar mass;  $s$  is the square of total energy in the over-all c.m. system;  $q$  is the momentum of incoming  $\pi$  in the over-all c.m. system;  $V$  is the total  $\pi_b^+\pi^-$  energy in their c.m. system ( $=\pi_b^+\pi^-$  effective mass);  $k_V$  is the momentum of  $\pi_b^+$  in  $\pi_b^+\pi^-$  system;  $W$  is the total  $p\pi_{a^+}$  energy in their c.m. system ( $=p\pi_{a^+}$  effective mass);  $k_W$  is the momentum of  $p$  in  $p\pi_{a^+}$  system;  $d\sigma_V/d\cos\vartheta$  is the differential cross section for elastic on-shell  $\pi^+\pi^-$  scattering;  $d\sigma_W/d\cos\Theta$  is the differential cross section for elastic on-shell  $p\pi^+$  scattering;  $F(\Delta^2)$  is the product of three form factors;  $g_V(V, \Delta^2)$  is the

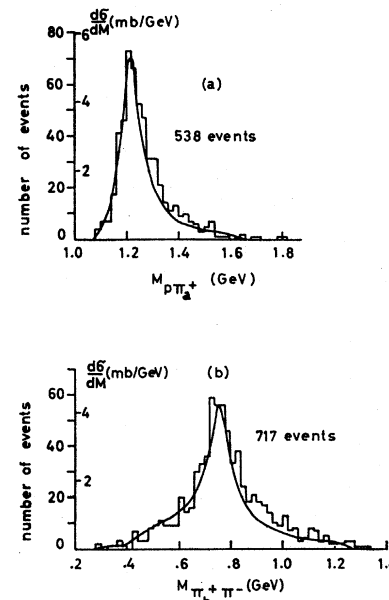
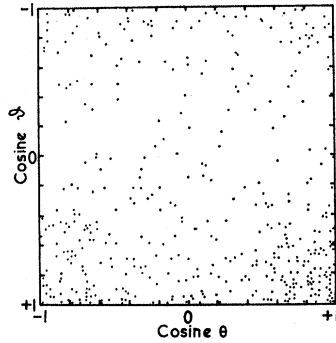


FIG. 17. Projection of (a)  $M_{p\rho a^+}$  from Fig. 16 for the  $\rho$  band (0.66 to 0.86 GeV) and of (b)  $M_{\pi_b^+\pi^-}$  for the  $N^*$  band (1.12 to 1.32 GeV). The curves show the OPE predictions.

<sup>27</sup> E. Ferrari, F. Selleri: Nuovo Cimento 21, 1028 (1961); *ibid.* Suppl. 24, 453 (1962); 27, 1450 (1963).

FIG. 18. Scatter diagram of the cosine of the angle  $\vartheta$  between incoming  $\pi^+$  and outgoing  $\pi_b^+$  in the  $\rho$  system versus the cosine of the angle  $\Theta$  between incoming and outgoing proton in the  $N^*$  system for events in the  $N^*\rho$  overlap region of Fig. 16.



off-shell correction function for the  $\pi_b^+\pi^-$  vertex;  $g_W(W, \Delta^2)$  is the off-shell correction function for the  $p\pi_a^+$  vertex.

In applying formula (1) for  $d\sigma_W/d\cos\Theta$  the experimental data of Lach<sup>28</sup> and of Helland *et al.*<sup>29</sup> on  $p\pi^+$  scattering have been used up to  $W=2.1$  GeV. Above 2.1 GeV an exponential expression has been adopted for the angular distribution. For  $d\sigma_V/d\cos\vartheta$  the best experimental information on the elastic  $\pi^+\pi^-$  scattering cross section and on the angular distribution (both as

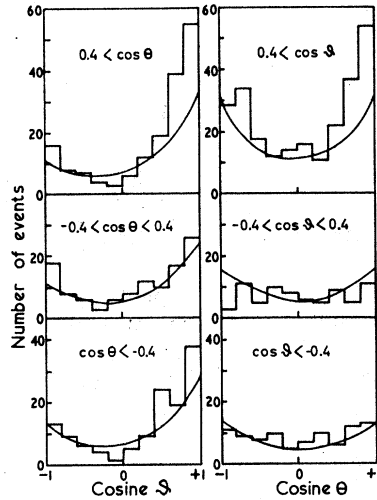


FIG. 19. Projections of  $\cos\Theta$  for 3 regions of  $\cos\vartheta$  and of  $\cos\vartheta$  for 3 regions of  $\cos\Theta$  from Fig. 18.

functions of  $V$ ) contained in the literature<sup>4,16(d),30,31</sup> has been used.

The following off-shell corrections have been used:

$$g_V(V, \Delta^2) = [k_V^{\text{off}}/k_V]^{2l}$$

with

$$k_V^{\text{off}} = [((V^2 + \mu^2 + \Delta^2)/2V)^2 - \mu^2]^{1/2}.$$

$l$  was taken to be 1 for  $0.45 \text{ GeV} < V < 1.16 \text{ GeV}$  since  $\rho$  production is the dominant process there. Above 1.16

<sup>28</sup> J. T. Lach, University of California Radiation Laboratory Report UCRL-10718, 1963 (unpublished).

<sup>29</sup> J. A. Helland, T. J. Devlin, D. E. Hagge, M. J. Longo, B. J. Moyer, and C. D. Wood, Phys. Rev. 134, B1062 (1964).

<sup>30</sup> Y. Y. Lee, University of Michigan, Technical Report 04938-1-T, 1964 (unpublished).

<sup>31</sup> G. Wolf, University of Hamburg, thesis, 1964 (unpublished).

GeV,  $l=2$  has been assumed because of the  $f$  meson. For  $W$  in the  $N^*$  region ( $W < 1.43 \text{ GeV}$ ),

$$g_W(W, \Delta^2) = \left(1 + \frac{\Delta^2 + \mu^2}{4m^2}\right) \left(1 + 3 \frac{\Delta^2 + \mu^2}{2m(M^* - m)}\right)^2 \times \left(1 + \frac{\Delta^2 + \mu^2}{2m(M^* - m)}\right)^{-6} \left[\frac{k_W^{\text{off}}}{k_W}\right]^2$$

with

$$k_W^{\text{off}} = \left[\left(\frac{W^2 + m^2 + \Delta^2}{2W}\right)^2 - m^2\right]^{1/2}$$

and

$$F(\Delta^2) = 3.40 \mu^2 / (\Delta^2 + 5.73 \mu^2) + 0.28 \text{ (see Ref. 24)}$$

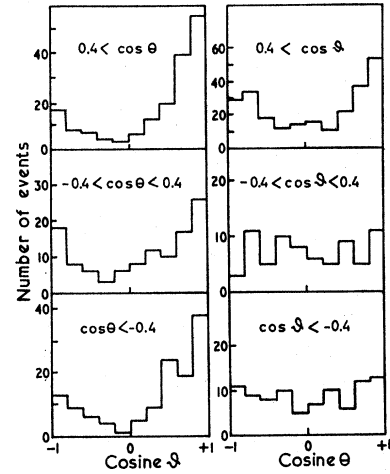


FIG. 20. The same as Fig. 19 with all distributions normalized to the same area.

has been adopted. For  $W$  outside the  $N^*$  region

$$|F(\Delta^2)|^2 g_W(W, \Delta^2) = [1 + (\Delta^2 + \mu^2)/90\mu^2]^{-2}$$

was taken.<sup>27</sup>

For the numerical application of formula (1) a program written by Söding has been used. This program constructs events of type (6) by a Monte Carlo method. Each event is then weighted according to formula (1). With this method the theoretical prediction for any experimental distribution of reaction (6) can be calculated, since it is also possible to compute quantities for systems involving particles from different vertices. (For instance in the case of the  $p\pi^+$  effective-mass distribution both  $p\pi^+$  masses were calculated for each Monte Carlo event.) Since there is no free parameter in formula (1), the calculation gives predictions which are *absolute* in magnitude.

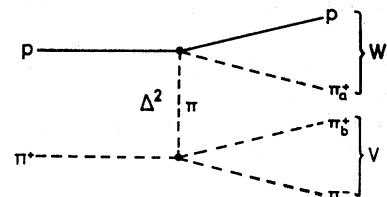


FIG. 21. OPE diagram for reaction  $\pi^+p \rightarrow p\pi^+\pi^+\pi^-$ .

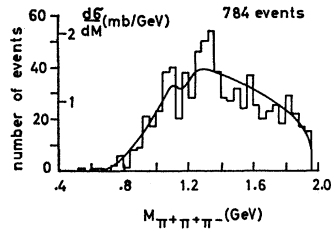


FIG. 22.  $\pi^+\pi^+\pi^-$  effective-mass distribution for reaction  $\pi^+p \rightarrow p\pi^+\pi^+\pi^-$  with both  $M_{p\pi^+}$  outside the  $N^*$  region (1.12 to 1.32 GeV). The curve shows the OPE prediction.

The curves shown in the effective mass distributions of Figs. 9, 12, and 17, in the  $\Delta^2$  distribution of Fig. 11 and in the angular distributions of Figs. 15 and 19 were calculated by the above method. The agreement is surprisingly good especially for Fig. 9 in view of the fact that no selection of low  $\Delta^2$  events has been made there. Thus it is clear that all the features of reaction (6) so far discussed, except for the correlations in Figs. 18–20, can be adequately explained by the OPE model. Under these circumstances it is important to see if the model can also account for any other prominent features of reaction (6). This will be discussed in the following sections.

### F. $\rho\pi$ Systems

We have previously presented evidence for two peaks ( $A_1$  and  $A_2$ ) in the  $\pi^+\rho^0$  effective mass distribution<sup>17(a)</sup> similar to those found in other experiments.<sup>9,12</sup> Figure 22 shows the  $\pi^+\pi^+\pi^-$  effective-mass distribution for events of type (6) with both  $M_{p\pi^+}$  outside the  $N^*$  region.

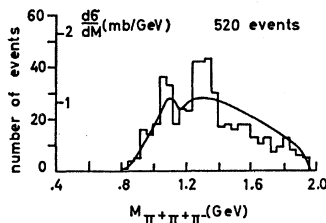


FIG. 23.  $\pi^+\pi^+\pi^-$  effective-mass distribution for reaction  $\pi^+p \rightarrow p\pi^+\pi^+\pi^-$  with both  $M_{p\pi^+}$  outside the  $N^*$  region and at least one  $\pi^+\pi^-$  combination in the  $\rho$  region (0.64 to 0.86 GeV). The curve shows the OPE prediction.

Figure 23 shows the same effective-mass distribution with the further restriction that at least one  $\pi^+\pi^-$  mass lies in the  $\rho$  region. If the  $A_1$  and  $A_2$  peaks represent real particles they cannot of course be produced by OPE. However, since the OPE model predicts other features of reaction (6) so successfully, we have used it to calculate its theoretical predictions for Figs. 22 and 23. In both figures these predictions are shown by the curves. These curves reproduce the general shape of the distributions quite well except for the  $A_2$  region. In the  $A_1$  region the OPE model gives a peak which, however, is not as narrow and as high as the experimental one. Deck<sup>32</sup> has already tried to explain the  $A_1$  enhancement as a kinematic consequence of the OPE model. In order to examine further if the  $A_1$  enhancement can indeed be explained by OPE we have calculated the angle  $\vartheta$  between incoming  $\pi^+$  and outgoing

$\pi^+(\pi_b^+)$ , which together with the  $\pi^-$  is in the  $\rho$  mass region in the  $\pi_b^+\pi^-$  system. For “double- $\rho$  events” both angles have been taken. Figure 24 shows the angular distributions for (a) the  $A_1$  and (b) the  $A_2$  region of Fig. 23 together with the curves computed from the OPE model. There is a marked difference between the experimental distributions for the two

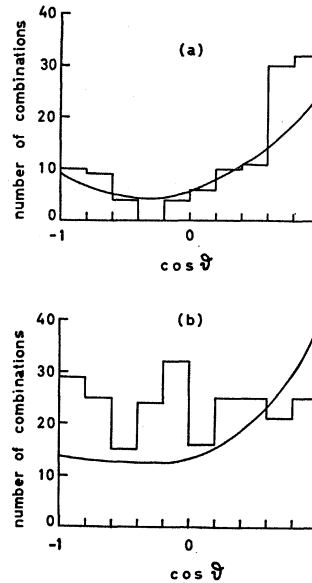


FIG. 24. Distribution of the angle  $\vartheta$  between incoming  $\pi^+$  and outgoing  $\pi^+$  from  $\rho$  decay in the  $\rho$  rest system for events (a) in the  $A_1$  region (1.02 to 1.14 GeV) and (b) in the  $A_2$  region (1.22 to 1.42 GeV) of Fig. 23. The curves show the OPE predictions.

cases, whereas the theoretical OPE predictions are rather similar. In the  $A_1$  region the observed forward backward asymmetry is reproduced well by the OPE curve.

The Chew-Low plot already published<sup>17(a)</sup> [ $M_{\rho\pi}^2$  versus  $\Delta^2(p/p)$ ] shows a marked difference between the  $\Delta^2(p/p)$  distribution for the  $A_1$  and  $A_2$  regions. These two  $\Delta^2(p/p)$  distributions up to 1 GeV<sup>2</sup> are

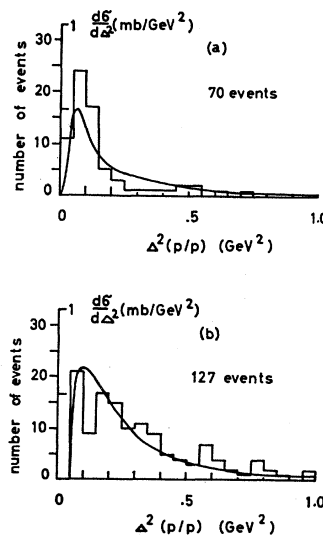


FIG. 25. Distribution of  $\Delta^2(p/p)$  for events (a) in the  $A_1$  region and (b) in the  $A_2$  region of Fig. 23. The curves show the OPE predictions.

<sup>32</sup> R. T. Deck, Phys. Rev. Letters 13, 169 (1964).

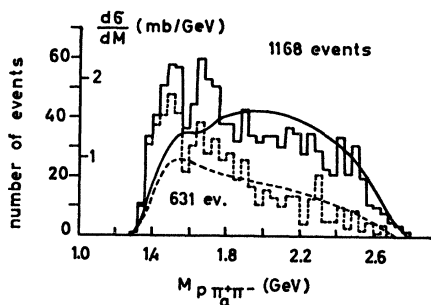


FIG. 26.  $p\pi_a^+\pi^-$  effective-mass distribution for reaction  $\pi^+p \rightarrow p\pi^+\pi^+\pi^-$  with  $1.12 \text{ GeV} < M_{p\pi_a^+} < 1.32 \text{ GeV}$ . "Double  $N^*$  events" were not taken. The dashed histogram is for events with  $\Delta^2(p/p\pi_a^+\pi^-) < 0.3 \text{ GeV}^2$ . The curves show the OPE predictions. "ev." = "events."

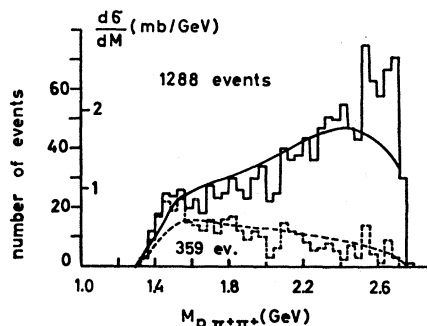


FIG. 27.  $p\pi^+\pi^+$  effective-mass distribution for reaction  $\pi^+p \rightarrow p\pi^+\pi^+\pi^-$  with at least one  $M_{p\pi^+}$  in the  $N^*$  region. The dashed histogram is for events with  $\Delta^2(p/p\pi^+\pi^+) < 0.3 \text{ GeV}^2$ . The curves show the OPE predictions. "ev." = "events."

shown in Fig. 25 together with the OPE predictions. The steep slope observed for the  $A_1$  region is reasonably well reproduced by the calculated curve; the distribution in the  $A_2$  region is much flatter.

In conclusion it appears that the OPE model is able

to describe reasonably well the general feature of the events in the  $A_1$  region, except for the height and the narrow width of the  $A_1$  enhancement. Thus we cannot draw a definite conclusion as to whether this enhancement represents a real particle or not.

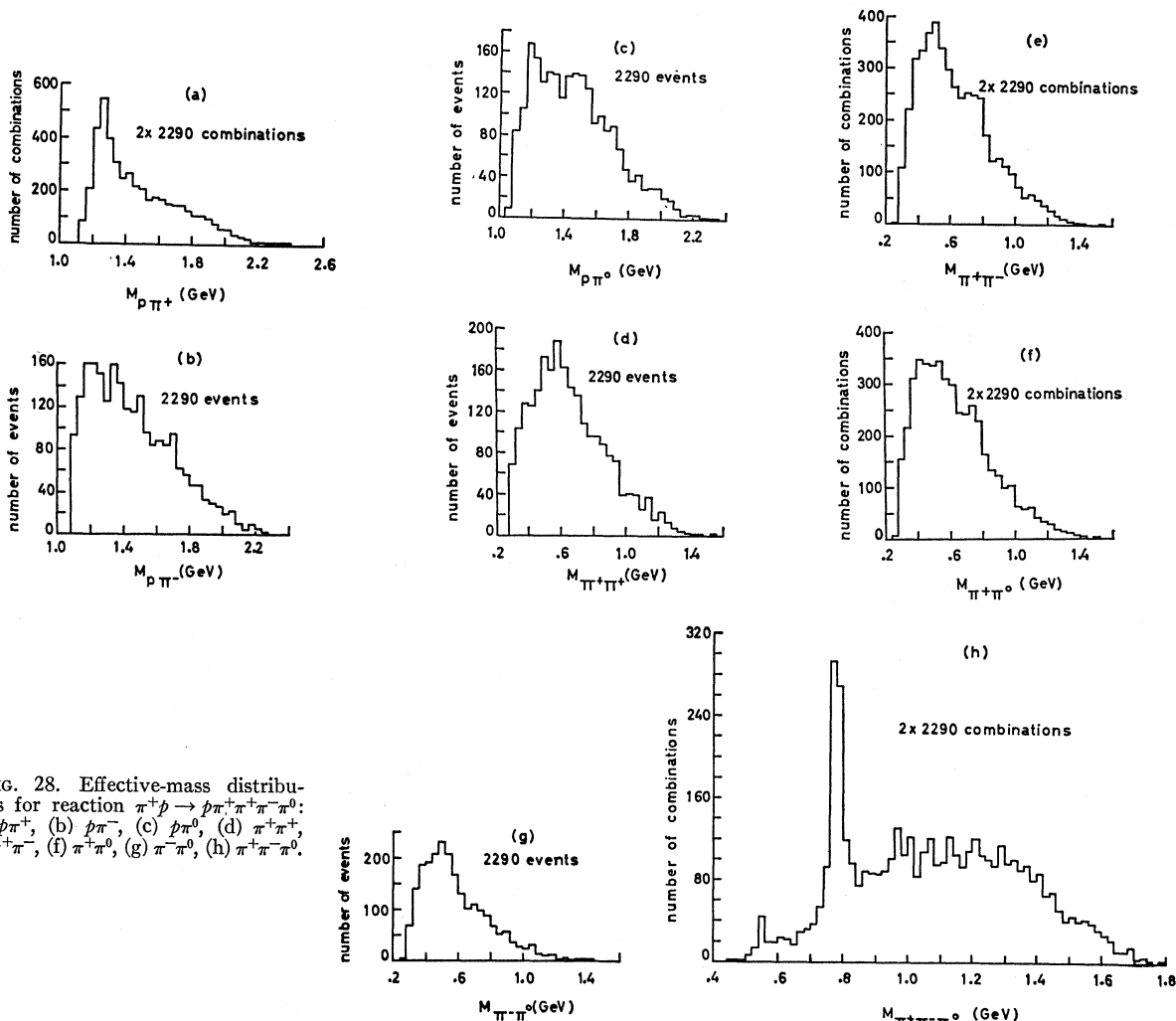


FIG. 28. Effective-mass distributions for reaction  $\pi^+p \rightarrow p\pi^+\pi^+\pi^-\pi^0$ : (a)  $p\pi^+$ , (b)  $p\pi^-$ , (c)  $p\pi^0$ , (d)  $\pi^+\pi^+$ , (e)  $\pi^+\pi^-$ , (f)  $\pi^+\pi^0$ , (g)  $\pi^-\pi^0$ , (h)  $\pi^+\pi^-\pi^0$ .

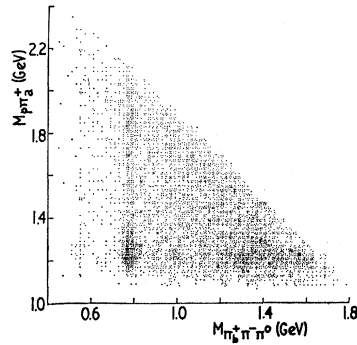


FIG. 29. Scatter diagram of  $M_{p\pi_a^+}$  versus  $M_{\pi_b^+\pi^-\pi^0}$  (two points per event) for reaction  $\pi^+p \rightarrow p\pi^+\pi^+\pi^-\pi^0$ .

The  $A_2$  in Figs. 22 and 23 stands out very clearly above the calculated curves. We have not tried to study the  $A_2$  production mechanism by the Gottfried-Jackson analysis<sup>20,33</sup> since removal of  $N^*$  events would bias the  $A_2$  decay angular distributions and without  $N^*$  removal the background is much too high.

### G. Higher Isobars

Figure 26 shows the  $p\pi_a^+\pi^-$  effective-mass distribution for events of type (6) with  $M_{p\pi_a^+}$  in the  $N^*$  region. If both  $p\pi^+$  combinations fell into the  $N^*$  region the event was not taken (for those events both  $p\pi^+\pi^-$  masses are above 2 GeV). The dashed histogram shows only events with  $\Delta^2(p/p\pi_a^+\pi^-) < 0.3 \text{ GeV}^2$ . The curves show the predictions of the OPE model. The model accounts reasonably well for the observed distribution in the high-mass region, but at lower masses there are two prominent peaks at 1.51 and 1.68 GeV. These peaks also show up in the over-all  $p\pi^+\pi^-$  mass distribu-

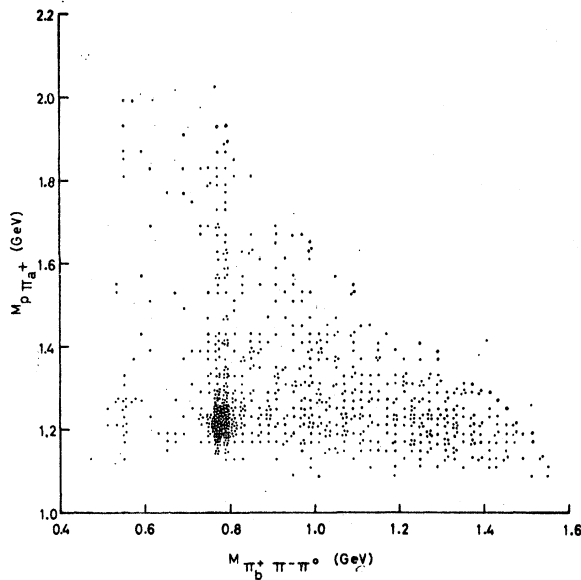


FIG. 30. Scatter diagram of  $M_{p\pi_a^+}$  versus  $M_{\pi_b^+\pi^-\pi^0}$  for reaction  $\pi^+p \rightarrow p\pi^+\pi^+\pi^-\pi^0$  with  $\Delta^2(p/p\pi_a^+) < 0.6 \text{ GeV}^2$ .

TABLE V. Partial cross sections for reaction (7).

Channel	$\sigma$ (mb)
(a) $p\pi^+\pi^+\pi^-\pi^0$ (no resonances)	1.0
(b) $N^{*++}\pi^+\pi^-\pi^0$	1.1
(c) $N^{*++}\omega^0$ ( $\omega^0 \rightarrow \pi^+\pi^-\pi^0$ )	0.35
(d) $N^{*++}\eta^0$ ( $\eta^0 \rightarrow \pi^+\pi^-\pi^0$ )	0.03
(e) $N^{*++}\pi\rho$	0.15
(f) $p\pi\pi\rho$	0.1
(g) $p\pi^+\eta^0$ ( $\eta^0 \rightarrow \pi^+\pi^-\pi^0$ )	0.04
(h) $N^{*++}H$	0.15
(i) $p\pi^+\omega^0$ ( $\omega^0 \rightarrow \pi^+\pi^-\pi^0$ )	0.5
$p\pi^+\omega^0$ (no $\omega\pi$ resonance)	0.4
$pB^+$	0.1

tion of Fig. 9(f) and may be identified with the two known  $T = \frac{1}{2}$  resonances at 1.52 and 1.69 GeV seen in

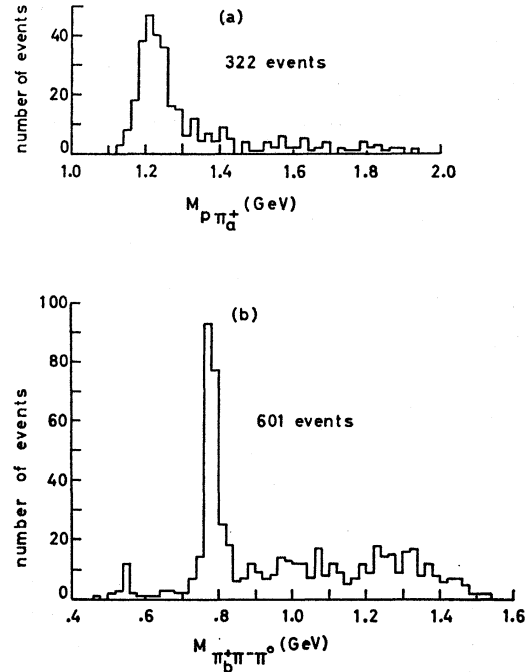


FIG. 31. Projection of (a)  $M_{p\pi_a^+}$  from Fig. 30 for the  $\omega$  band (0.74 to 0.84 GeV) and of (b)  $M_{\pi_b^+\pi^-\pi^0}$  for the  $N^*$  band (1.12 to 1.32 GeV).

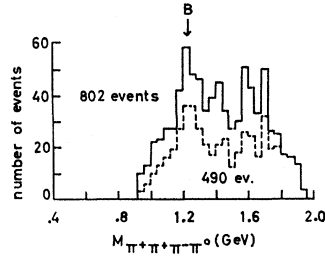
pion-nucleon elastic scattering. As pointed out in Sec. 3B the peaks also appear in the  $N\pi$  system (Fig. 2).

Figure 27 shows the  $p\pi^+\pi^+$  effective-mass distribution for reaction (6) with at least one  $M_{p\pi^+}$  in the  $N^*$  region; the dashed histogram is for events with  $\Delta^2(p/p\pi^+\pi^+) < 0.3 \text{ GeV}^2$ . The curves show the OPE predictions. Again a good agreement is observed except for the highest mass region of the solid histogram. The excess of events there is a direct kinematical consequence of the abundance of events at low  $p\pi_a^+\pi^-$  masses in Fig. 26. For low  $\Delta^2$  there is also a small number of events above the predicted curve for  $p\pi^+\pi^+$  masses below 1.6 GeV.

We have also examined the  $p\rho^0$  effective-mass distribution by plotting  $M_{p\pi_c^+\pi^-}$  for events with  $M_{p\pi_a^+}$

<sup>33</sup> J. D. Jackson, Nuovo Cimeno 34, 1644 (1964).

FIG. 32.  $\pi^+\pi^+\pi^-\pi^0$  effective-mass distribution for reaction  $\pi^+p \rightarrow p\pi^+\pi^+\pi^-\pi^0$  with at least one  $\pi^+\pi^-\pi^0$  combination in the  $\omega$  region (0.74 to 0.84 GeV). The dashed histogram is for events with  $\pi_b^+\pi^-\pi^0$  in the  $\omega$  region and  $p\pi_a^+$  outside the  $N^*$  region. "ev." = "events."



outside the  $N^*$  region and  $M_{\pi_b^+\pi^-}$  in the  $\rho$  region. No enhancement was observed.

5. REACTION  $\pi^+p \rightarrow p\pi^+\pi^+\pi^-\pi^0$

A. Effective-Mass Distributions and Cross Sections

Figure 28 shows the effective-mass distributions for all two-particle systems and for the  $\pi^+\pi^-\pi^0$  system of the reaction

$$(7) \quad \pi^+p \rightarrow p\pi^+\pi^+\pi^-\pi^0.$$

The partial cross sections for this channel are listed in Table V.

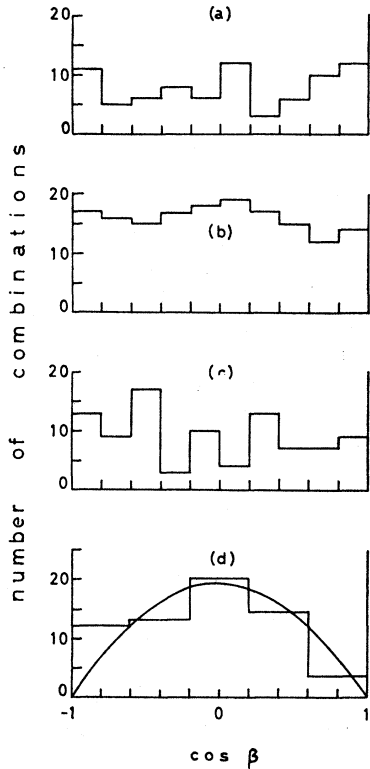


FIG. 33. Distribution for  $\cos\beta$ , where  $\beta$  is the angle between  $\pi_a^+$  and the normal to the " $\omega$ " (i.e.,  $\pi_b^+\pi^-\pi^0$ ) decay plane in the  $\pi_b^+\pi^-\pi^0$  c.m. system for reaction  $\pi^+p \rightarrow p\pi^+\pi^+\pi^-\pi^0$  with  $M_{\pi_b^+\pi^-\pi^0}$  in the  $\omega$  region and  $M_{p\pi_a^+}$  outside the  $N^*$  region. If both  $M_{\pi_b^+\pi^-\pi^0}$  were in the  $\omega$  region and both  $M_{p\pi_a^+}$  outside the  $N^*$  region both angles have been taken. (a)  $0.96 \text{ GeV} < M_{\pi^+\pi^+\pi^-\pi^0} < 1.16 \text{ GeV}$ , (b)  $1.16 \text{ GeV} < M_{\pi^+\pi^+\pi^-\pi^0} < 1.36 \text{ GeV}$  ( $B$  region), (c)  $1.36 \text{ GeV} < M_{\pi^+\pi^+\pi^-\pi^0} < 1.56 \text{ GeV}$ . (d) shows the  $\cos\beta$  distribution for the  $B$  region after background subtraction.

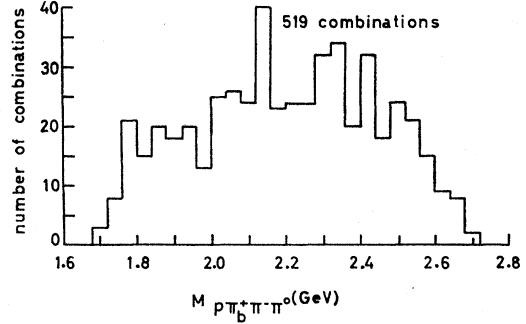


FIG. 34.  $p\pi_b^+\pi^+\pi^-\pi^0$  effective-mass distribution for reaction  $\pi^+p \rightarrow p\pi^+\pi^+\pi^-\pi^0$  with  $M_{\pi_b^+\pi^-\pi^0}$  in the  $\omega$  region and  $M_{p\pi_a^+}$  outside the  $N^*$  region.

B.  $N^{*++}$  and  $\omega$  Production

Figure 28 shows that, as at lower energies,<sup>3</sup> there is strong production of  $N^{*++}$  and  $\omega$ . However, whereas at the lower energies the reaction

$$(7c) \quad \pi^+p \rightarrow N^{*++}\omega^0$$

dominates, at our energy only about half the  $\omega$  mesons are produced together with an  $N^{*++}$ . This is demonstrated by Fig. 29 which shows  $M_{p\pi_a^+}$  versus  $M_{\pi_b^+\pi^-\pi^0}$  (2 points per event).

We have investigated the reaction (7c) in a previous publication<sup>17(g)</sup> in an attempt to determine the production mechanism. For this analysis a highly pure sample of the reaction was obtained by restriction to events with  $\Delta^2(p/p\pi_a^+) < 0.6 \text{ GeV}^2$ . Figure 30 shows  $M_{p\pi_a^+}$  versus  $M_{\pi_b^+\pi^-\pi^0}$  for events satisfying this  $\Delta^2$  restriction. The projections of  $M_{p\pi_a^+}$  for the  $\omega$  band (0.74 to 0.84 GeV) of Fig. 30 and the projection of  $M_{\pi_b^+\pi^-\pi^0}$  for the  $N^*$  band are shown in Fig. 31. As can be seen there is very little background left in the resonance regions. The analysis carried out in Ref. 17(g) showed that the

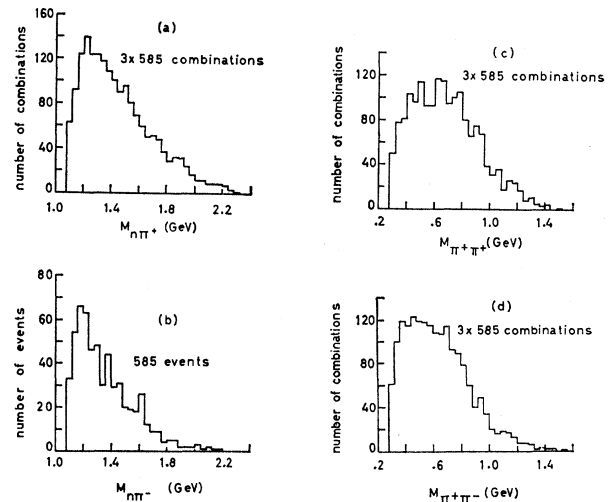


FIG. 35. Effective mass distributions for reaction  $\pi^+p \rightarrow n\pi^+\pi^+\pi^-\pi^-$ : (a)  $n\pi^+$ , (b)  $n\pi^-$ , (c)  $\pi^+\pi^+$ , (d)  $\pi^+\pi^-$ .

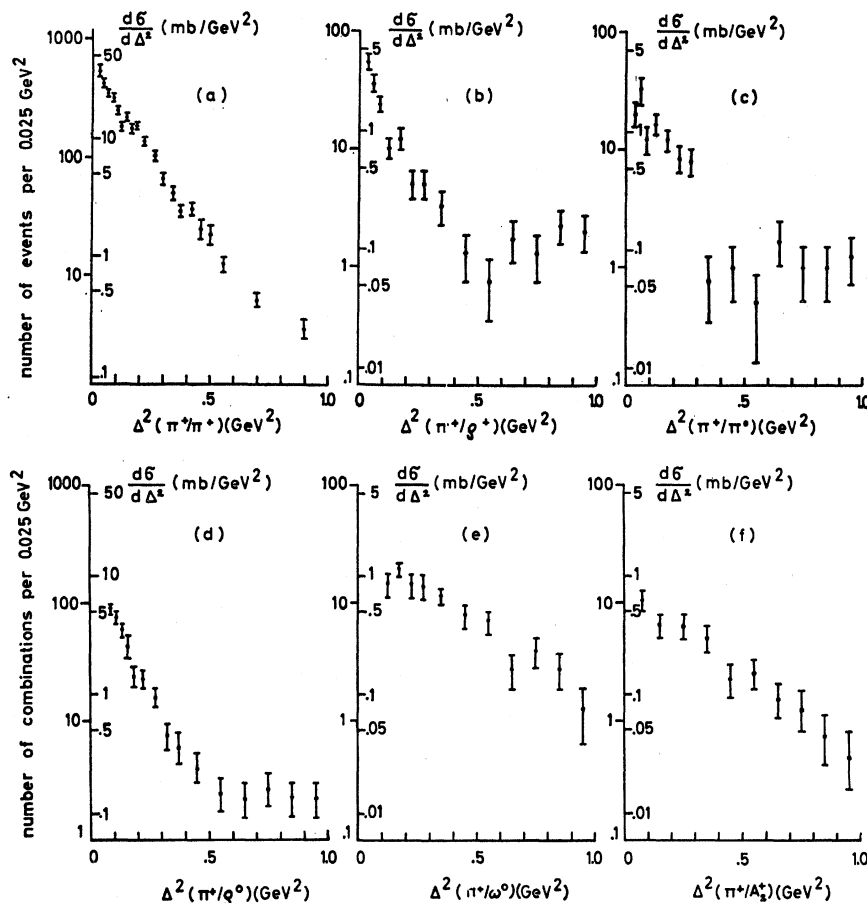


FIG. 36.  $\Delta^2$  distributions for reaction (a)  $\pi^+p \rightarrow p\pi^+$ , (b)  $\pi^+p \rightarrow p\rho^+$ , (c)  $\pi^+p \rightarrow N^{*+}\pi^0$ , (d)  $\pi^+p \rightarrow N^{*+}\rho^0$ , (e)  $\pi^+p \rightarrow N^{*+}\omega^0$ , (f)  $\pi^+p \rightarrow pA_2^+$  for small  $\Delta^2$  ( $\Delta^2 < 1.0$  GeV $^2$ ).

experimental results for reaction (7c) are not in agreement with the theoretical predictions for  $\rho$  exchange without absorptive effects ( $\pi, f, \eta$ , and  $\omega$  exchanges are of course forbidden for this reaction). However, if one includes absorption in the theoretical calculations,<sup>34</sup> the experimental data may be consistent with the predictions for  $\rho$  exchange.

### C. B Meson

Not all  $\omega$  mesons are produced together with an  $N^*$ . So we have looked for  $B$ -meson production by plotting in Fig. 32 the  $\pi^+\pi^+\pi^-\pi^0$  effective-mass distribution for events with at least one  $\pi^+\pi^-\pi^0$  combination in the  $\omega$  mass region (solid histogram). The  $B$  meson (1215 MeV) does show up in this distribution. In order to remove background events we also show the  $\pi^+\pi^+\pi^-\pi^0$  mass distribution (dashed histogram) for events with  $M_{\pi_b^+\pi^-\pi^0}$  in the  $\omega$  region and  $M_{p\pi_a^+}$  outside the  $N^*$  region.

In spite of the high ratio of background to  $B$  mesons (about one-to-one) an attempt has been made to determine the spin and parity of  $B$ . For this purpose we have plotted in Fig. 33 the cosine of the angle  $\beta$

between the  $\omega$ -decay-plane normal and the direction of  $\pi_a^+$  in the  $\omega$  (i.e.,  $\pi_b^+\pi^-\pi^0$ ) rest system for the following intervals of  $M_{\pi^+\pi^+\pi^-\pi^0}$ : (a) 0.96 to 1.16 GeV, (b) 1.16 to 1.36 GeV ( $B$  region), (c) 1.36 to 1.56 GeV. Figure 33(d) shows the  $\cos\beta$  distribution for the  $B$  region after subtraction of a distribution obtained from the adjacent regions (a) and (c) and normalized to the background under the  $B$ . From angular momentum and parity conservation in the  $B$  decay it follows that  $\cos\beta$  should be distributed proportionally to  $\sin^2\beta$  if the  $B$  has natural parity [ $P = (-1)^J$ ]. For  $J^P = 0^-$  one expects a  $\cos^2\beta$  distribution; for the other unnatural parities the angular distribution is undetermined. The distribution of Fig. 33(d) is consistent with  $\sin^2\beta$  (as shown by the curve) but not with  $\cos^2\beta$  thus ruling out  $0^-$  ( $0^+$  is not possible for a particle decaying into  $\omega\pi$ ).

We have also tried to apply the method proposed by Ademollo *et al.*<sup>35</sup> to determine the spin and parity of the  $B$  meson. In the  $B$  region the moments computed for our events were not internally consistent with the theoretical predictions for any  $J^P$  assignment. This inconsistency possibly arises from the strong back-

<sup>34</sup> B. Svensson (private communication).

<sup>35</sup> M. Ademollo, R. Gatto, and G. Preparata, Phys. Rev. Letters 12, 462 (1964).

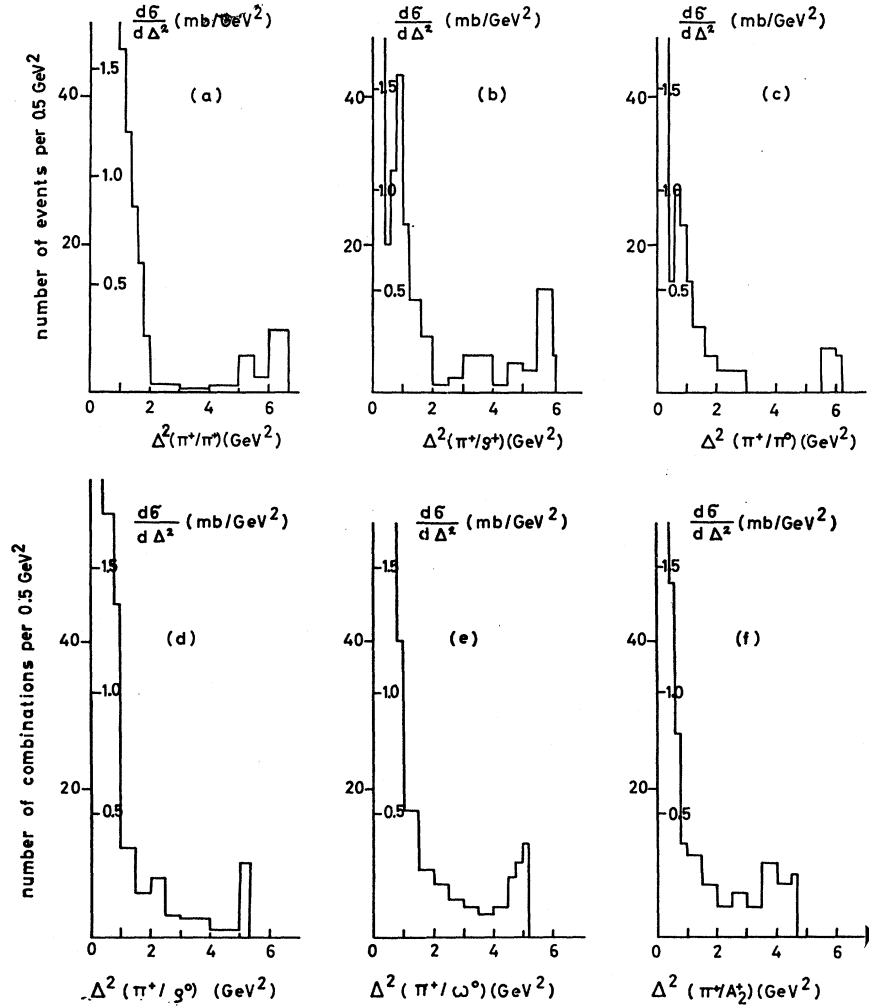


FIG. 37.  $\Delta^2$  distributions for the reactions listed in the caption to Fig. 36 for all  $\Delta^2$ .

ground the effect of which could not be taken into account.

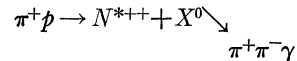
#### D. $\eta$ Meson

In Fig. 28(h) the  $\eta$  meson shows up quite clearly. From Fig. 29 it was found that in about 50% of the cases the  $\eta$  meson is produced together with an  $N^*$  (see Table V).

#### E. $\rho\pi$ System

As pointed out in a previous publication,<sup>17(e)</sup> relatively few  $\rho$  mesons are produced in reaction (7) (see Fig. 28), but those that appear to occur in association with an  $N^*$ . In Ref. 17(e) these events were analyzed in detail and evidence was presented for a  $\rho\pi$  enhancement at 0.975 GeV. We have made sure that this peak in the  $\pi_b^+\pi^-\pi^0$  mass distribution is not a kinematical reflection from those events, for which  $\pi_a^+\pi^-\pi^0$  is in the  $\omega$  region. Since<sup>36</sup> the mass value of

0.975 GeV is so close to that of the  $X^0$  the question arises whether the enhancement might be due to the reaction



where the events have been incorrectly fitted to the hypothesis with a  $\pi^0$  instead of a  $\gamma$ . To check this we have fitted the events in the region of the enhancement to the hypothesis  $\pi^+p \rightarrow p\pi^+\pi^-\pi^-\gamma$ . For events giving a good fit we have plotted the  $\pi_b^+\pi^-\gamma$  effective-mass distribution if  $M_{p\pi_a^+}$  was in the  $N^*$  region. There was no peak at 0.96 GeV, the mass of the  $X^0$ . Furthermore the previously published<sup>17(e)</sup> missing-mass distribution for events of the type  $\pi^+p \rightarrow N^{*++} + \text{neutrals}$  also does not show any peak at the  $X^0$  mass, though it should if the reaction  $\pi^+p \rightarrow N^{*++} + X^0$  really did occur since the  $X^0$  decays into neutrals about 50% of the time.<sup>36</sup>

<sup>36</sup> G. R. Kalbfleisch, L. W. Alvarez, A. Barbaro-Galtieri, O. I. Dahl, P. Eberhard *et al.*, Phys. Rev. Letters 12, 527 (1964);

M. Goldberg, M. Gundzik, S. Lichtman, J. Leitner, M. Primer, *et al.*, *ibid.* 12, 546 (1964); M. Goldberg, M. Gundzik, J. Leitner, M. Primer, P. L. Connolly, *et al.*, *ibid.* 13, 249 (1964).

### F. Search for Other Resonances

In order to search for a possible  $p\omega$  peak, we have plotted in Fig. 34 the  $p\pi_b^+\pi^-\pi^0$  effective-mass distribution for reaction (7) with  $M_{\pi_b^+\pi^-\pi^0}$  in the  $\omega$  region (0.74 to 0.84 GeV) and  $M_{p\pi_a^+}$  outside the  $N^*$  region. There is no statistically significant enhancement in this distribution.

In the  $p\pi\pi$  effective-mass distributions there was no clear evidence for the higher isobars.

#### 6. REACTION $\pi^+p \rightarrow n\pi^+\pi^+\pi^+\pi^-$

Figure 35 shows the effective-mass distributions for all two-particle systems in the reaction

$$(8) \quad \pi^+p \rightarrow n\pi^+\pi^+\pi^+\pi^-.$$

There appears to be very little resonance production in this channel; only the  $N^{*-}$  shows up clearly, corresponding to a cross section of 0.25 mb for  $\pi^+p \rightarrow N^{*-}\pi^+\pi^+\pi^+$ . There might also be a slight amount of  $N^{*+}$  and  $\rho^0$  production, but because there are three positive pions per event the  $n\pi^+$  and  $\pi^+\pi^-$  mass distributions contain a very high proportion of background.

#### 7. REACTIONS $\pi^+p \rightarrow p\pi^+\pi^+\pi^-(m\pi^0)$ AND $\pi^+p \rightarrow n\pi^+\pi^+\pi^+\pi^-(m\pi^0)$

In the effective-mass distributions for these channels there was no indication for resonance production except for some  $N^{*++}$ .

### 8. $\Delta^2$ DISTRIBUTIONS FOR TWO-BODY REACTIONS

From the previous discussion it is clear that two-body processes play an important role in the studied reactions. In the following we compare the  $\Delta^2$  distributions for the channels

- (a)  $\pi^+p \rightarrow p\pi^+$ ,
- (b)  $\pi^+p \rightarrow p\rho^+$ ,
- (c)  $\pi^+p \rightarrow N^{*++}\pi^0$ ,
- (d)  $\pi^+p \rightarrow N^{*++}\rho^0$ ,
- (e)  $\pi^+p \rightarrow N^{*++}\omega^0$ ,
- (f)  $\pi^+p \rightarrow pA_2^+$ .

Figure 36 shows on a logarithmic scale the distributions of the momentum transfer  $\Delta^2$  for these channels for the  $\Delta^2$  range up to 1 GeV<sup>2</sup>. The reactions (b), (c), and (d) are all characterized by a sharp falloff up to a  $\Delta^2$  of 0.5 GeV<sup>2</sup>. This falloff is nearly the same as that for the elastic scattering (a). Reactions (e) and (f) have a much slower decrease with  $\Delta^2$ . In Fig. 37 the  $\Delta^2$  distributions are shown for the whole kinematical range for each reaction on a linear scale. They all appear to be characterized by a small accumulation of events in the highest  $\Delta^2$  region. This accumulation persists after background subtraction, as has been checked by using the appropriate Chew-Low plots.

### ACKNOWLEDGMENTS

We are very much indebted to the staff of the CERN Proton Synchrotron and to the crews of the Saclay hydrogen bubble chamber. The help of our scanning and measuring teams has been invaluable. Those groups (Aachen, Bonn, Hamburg, London, München) which used the GRIND fitting program thank the CERN Data Processing Division. The Birmingham group is grateful to the programming team of NIRNS.

All groups are grateful to the computer staff of DESY (in particular to Dr. Lublow) for the final compilation of the data with ULTRAN. We also thank the Institut für experimentelle Mathematik at Bonn, the Deutsches Rechenzentrum at Darmstadt and the Institut für Plasmaphysik at München for computer time.

The Imperial College group is indebted to L. M. Celnikier for his continued assistance in programming. One member (F.C.) gratefully acknowledges financial support by the Government of British Guiana.

The British groups have been supported in part by a grant from the Department of Scientific and Industrial Research. The groups of Aachen, Bonn, Hamburg and München acknowledge financial support from the Bundesministerium für Wissenschaftliche Forschung.